Journal of Materials Chemistry A

ROYAL SOCIETY OF CHEMISTRY

PAPER

View Article Online
View Journal | View Issue

Cite this: J. Mater. Chem. A, 2024, 12, 26280

An insight into separating H_2 from natural gas/H_2 mixtures using Mg-based systems†

Mateusz Balcerzak, *[abc] Robert Urbanczyk, [ad] Fabian Lange,[a] Francis Anne Helm,[a] Jan Ternieden [a] and Michael Felderhoff [a]

The use of light, abundant, and relatively cheap Mg-based systems arouses great interest in hydrogen-economy-related applications such as hydrogen and heat storage. So far, MgH_2, capable of storing large amounts of H_2 (7.6 wt%), has been scarcely evaluated for its H_2 separation potential, which may be crucial for H_2 recovery from various H_2-containing gas mixtures. Herein, we reveal and discuss the ability of Mg-based systems to separate H_2 from CH_4-rich gas mixtures. Mg-Ni and Mg-Fe systems can separate ~5.5 wt% of H_2 during the hydrogenation process and release pure H_2 (at least 99.9%) within the dehydrogenation process. Pure H_2 can, therefore, be obtained in a one-step separation system. In this study, we discuss the selection of the hydrogenation/dehydrogenation processes catalyst (Ni, Fe) as well as the optimal separation process temperature. The tested systems show satisfactory performance stability during cyclic H_2 separation from CH_4/H_2 and natural gas/H_2 gas mixtures. We also present the first investigation of the Mg-based systems (with Ni or Fe catalyst) after the cycled separation processes. The results of complementary techniques revealed H_2 separation-induced chemical and phase segregation in the studied materials. Moreover, we report the observation of networked MgH_2 microstructure formation. This research points out the potential of metal-hydrides in the H_2 separation sector as well as the challenges facing their application – especially those related to the presence of CO_2 impurity in the gas mixture. The unique and detailed description of processes taking place in a reactor during the separation process will significantly impact the design of future metal-hydrides-based scaled-up systems for H_2 separation.

Received 12th August 2024
Accepted 2nd September 2024

DOI: 10.1039/d4ta05654j

rsc.li/materials-a

Introduction

Climate change, environmental pollution, and biodiversity loss are forcing humankind, the initiator of critical changes on Earth, to change its current way of life. Since the warnings contained in the Club of Rome report regarding the negative impact of CO_2 on the Earth's atmosphere, many Climate Change Conferences focus on putting pressure on countries worldwide to defossilize their economies. One option that is perceived as a game changer for the global economy is hydrogen (H_2).

The transformation to a hydrogen economy and its associated challenges can be followed by the example of Germany – a country transitioning to a zero-emission economy.[1] Considering the long-range H_2 transport sector in Germany, which connects the H_2 production sites with the end-use destinations, the total length of pipelines is planned to reach 9700 km by 2032 (Fig. S1†).[2] Approximately 60% of the mentioned total H_2 pipeline length will operate using currently available natural gas pipelines.[2] For this reason, to fulfill the transformation goals during the energy transition (towards the hydrogen economy), H_2 will be transported together (as a stable blend) with natural gas (NG). The transfer of NG/H_2 gas mixtures from North Africa to Europe utilizing the existing pipelines is also under consideration.[3] Intermediate solutions are also expected in many technology sectors, such as gas turbines, which require further development to enable the full transformation from operating on NG to pure H_2 (Fig. S2, Chapter S1 of the ESI†).

In most cases, the transport of H_2 blended in NG must be combined with its recovery at the end of the pipeline. Therefore, apart from the key sectors of the hydrogen economy (H_2 production, transport, storage, and end use), H_2 separation and purification are exceptionally important technologies that allow the merging of all the economic sectors. They not only enable

[a]Heterogeneous Catalysis Department, Max-Planck-Institut für Kohlenforschung, Kaiser-Wilhelm Platz 1, Mülheim an der Ruhr 45470, Germany. E-mail: balcerzak@kofo.mpg.de; Fax: +49 208 306 2995; Tel: +49 208 306 2344

[b]Hydrogen and Fuel Cell Center (ZBT), Carl-Benz-Straße 201, Duisburg 47057, Germany

[c]Institute of Materials Science and Engineering, Poznan University of Technology, Poznan 61-138, Poland

[d]F4 Gasprozesstechnik & Energieverfahrenstechnik, Institut für Umwelt & Energie, Technik & Analytik e. V., Bliersheimer Str. 58–60, Duisburg 47229, Germany

† Electronic supplementary information (ESI) available: Supporting figures and tables, additional characterization data and discussion. See DOI: https://doi.org/10.1039/d4ta05654j

the efficient H_2 production and safe operation of H_2-containing gas mixtures but are also crucial to supplying high-purity H_2 to the sectors and devices where the H_2 purity is critical – *e.g.*, fuel cells.[4–6]

There are many established H_2 separation/purification techniques: pressure swing adsorption (PSA),[4,5,7] temperature swing adsorption (TSA),[8–10] vacuum swing adsorption (VSA),[8,11] cryogenic separation,[12] membrane techniques,[13–16] and electrochemical compressors/separators (EHC/S).[17–20] All these methods have their advantages and disadvantages. For example, the PSA technique, which separates >99% pure H_2 is limited to operating at relatively high initial H_2 concentrations (75–90%).[21] Moreover, PSA, TSA, and VCA operate discontinuously. The cryogenic methods, whereas, are relatively expensive and deliver H_2 of only <98% purity.[12,22] The use of Pd-membranes, which show very good H_2 separation properties, is limited by the high cost of Pd. Moreover, these membranes suffer from low resistance to poisoning (by CO and H_2S) and high operating temperature (>300 °C).[13,23] Perovskite-based proton-conducting membranes are characterized by a low H_2 flux, are sensitive to gas impurities (CO_2 and H_2O), and their performance largely depends on their production method.[22] The H_2 separation selectivity of the polymeric membranes is limited,[24–26] and can only be improved using a complex two-step system combining polymeric membrane and PSA.[24,27] The EHC/S systems, can operate continuously and separate H_2 of relatively high purity (100–500 ppm CH_4 in H_2 on the cathode site). However, their restraint is the low H_2 yield (<90%) when a gas mixture with a low H_2 concentration is supplied at the anode site.[20]

An alternative to the H_2 separation methods discussed above are metals and alloys that can react with H_2, forming hydrides. The principle of metal hydride operation is based on the selective absorption of H_2 from the gas mixture used. While H_2 is chemically stored in the metallic structure, the other gas components remain unreacted in the initial gas mixture.[28] Separation using metal hydride-based systems does not involve a significant pressure drop, so no additional energy is needed to compress the residual gas. The selectivity of the metal hydride can be tuned by the selection of chemical composition, crystal structure, and operating temperature.

Several metallic systems (mostly from low-temperature, AB_5-type intermetallic compounds) have already been used to separate H_2 from various gas mixtures.[29,30] For example, $MmNi_{5-x}Al_x$ (where Mm stands for mishmetal) can effectively recover high-purity H_2 (grade 5.0) from the synthetic ammonia production plant's pre-treated purge gas (with lower ammonia and moisture content).[31] T. Saitou *et al.* showed that another low-temperature system – $FeTi_{0.95}Mm_{0.08}$ can also separate highly pure H_2 (grade 7.0) from CH_4-containing gas mixtures.[32] In another work, F. R. Block *et al.* revealed that $LaNi_5$ and FeTi could absorb H_2 from gas mixtures. However, different gas impurities such as CO, CO_2 and H_2S strongly poisoned the active material.[33] Currently, the most serious restraint of the use of metal hydrides in separation applications is the gaseous poisoning of the material initiated by gases like O_2, CO_2, or H_2O vapor, which leads to the partial or complete deactivation of the material (mostly through its surface passivation).[34–36]

Compared to low-temperature alloys (for example AB_5- and AB-type systems), high-temperature hydrides exhibit higher gravimetric H_2 storage capacities. The most studied representative of this group is MgH_2, which is considered cheap (3000 $/t Mg powder),[37] abundant, light, and capable of storing 6.0–7.6 wt% H_2.[38] Despite the potential of MgH_2 in H_2 separation applications being predicted in 1987, research on this topic is very limited.[39] S. Ono proved that Mg (catalyzed by Ni) separates large amounts of pure H_2 (grade 6.0) from H_2-containing gas mixtures.[40] In our recent study, we presented that a Mg-based system is capable of absorbing all of the provided H_2 from a limited volume of CH_4/H_2 (90 : 10) mixture.[41] Although B. Bogdanović *et al.* demonstrated the possibility of using Mg to separate H_2 from H_2/CH_4 gas mixtures, the experiments were never extended to NG/H_2 (especially to gas mixtures rich in NG).[39] In addition, the detailed analysis of the Mg-based material after the separation experiments, which is necessary for the final materials implementation, has never been presented.

Herein, we demonstrate and discuss, for the first time, the H_2 separation from CH_4-rich gas mixtures (including NG-based blends) using Mg catalyzed by different metals (Ni or Fe). To the best of our knowledge, the effect of Fe catalyst on Mg separation properties (in any H_2-containing blends) has never been addressed. Ni and Fe proved to be effective catalysts for hydrogenation/dehydrogenation reactions in Mg-based systems (when pure H_2 is used in the reaction).[42] Transition metals facilitate hydrogenation by accelerating the dissociation of H_2 molecules into the H atoms and dehydrogenation promoting H atoms diffusion between the subsurface and the surface (in the case of Mg-Ni system) and weakening the Mg-H interaction strength (in the case of Mg-Fe system).[43,44]

The influence of different processing temperatures on the system performance was also demonstrated. This work contains a detailed analysis of the metal hydride systems after cyclic separation processes (to our knowledge, this has not been reported for any system so far), providing unique insights into the processes occurring during H_2 recovery. Furthermore, since CH_4 does not react with Mg and Mg-based systems, it is crucial for the feasibility of this hydride-based system to check the impact of NG pollutants on the durability of the active material.[40,45] Therefore, in this study, we specifically focused on the influence of CO_2, which, according to the literature, can be adsorbed on the Mg particles' surface and then be reduced to CH_4, simultaneously causing Mg oxidation.[40] The highlighted advantages and challenges of Mg-based systems will be useful for the design of metal hydride-based systems for H_2 separation and purification.

Experimental

Materials and gases

Pure Mg (Non-Ferrum GmbH, <45 μm, 99.8% purity), Ni (Honeywell Riedel-de Haën, <45 μm, 99.8% purity), and Fe (Sigma Aldrich, <45 μm, 99.5% purity) powders were used in this study. The morphology of these powders is presented in Fig. S3.† Depending on the experiment, Mg-Ni or Mg-Fe powder

mixtures were used. Ni and Fe were applied as catalysts to improve the Mg hydrogenation/dehydrogenation kinetics.[39] The weight ratio of Mg to the second element equaled 95 : 5. The starting powders were mixed for one hour under Ar using SPEX 8000M mill (without milling balls). The mixing resulted in a fine blending of the elements and not in an alloy formation or amorphization of the shaken materials (Fig. S4†). To avoid oxidation, all the handling with materials before and after mixing or any experiments was done in the MBraun glovebox filled with purified argon atmosphere (O_2 and H_2O <1 ppm).

High-purity H_2, N_2, Ar, and CO_2 gases were used in all experiments (Air Liquide, grade 5.0). The CH_4 (grade 4.5) and natural gas – NG (Natural gas H) were purchased from Air Liquide. The composition of NG was evaluated/confirmed by mass spectrometry (MS) and gas chromatography (GC) – see Table S1, Fig. S5, and Chapter S2 in the ESI†. The CH_4/H_2, NG/H_2, and H_2/CO_2 gas mixtures were prepared on-site.

The CH_4/H_2 gas composition calibration curves were determined based on the results of GC performed on the gas mixtures well-determined in terms of composition (prepared on-site using the calibrated EL-FLOW Bronkhorst mass flow meters, with the accuracy of 0.01%) – see Fig. S6 and S7.† The linear and exponential fits were used for 5–15% and 75–95% CH_4 concentration in the CH_4/H_2 gas mixtures, respectively. The H_2 or CH_4 concentration calculations were based on the ratios between H_2 and CH_4 integrals. The calibration curves were used to evaluate the composition of the prepared on-site gas mixtures and the CH_4 concentration in the desorbed H_2.

Separation of H_2 from CH_4/H_2, NG/H_2 gas mixtures

The H_2 separation experiments were performed using the setup presented in Fig. S8.† Its detailed description can be found in Chapter S4 of the ESI†. A 100 mL autoclave and 500 mL reservoir were used in the gas separation experiments. The temperature of the reservoir was kept constant at 30 °C.

Before any experiments, the setup with a loaded autoclave (with one gram of Mg-Ni or Mg-Fe system) was evacuated several times under dynamic vacuum and purged with pure Ar at room temperature. The Mg-Ni and Mg-Fe systems were firstly hydrogenated (about ten times) under pure H_2 (20 bar H_2). These hydrogenation cycles were treated as activation of the material – to obtain a stable hydrogen storage capacity and good hydrogenation kinetics (the details are published elsewhere).[41] Next, the systems were used to separate H_2 from CH_4/H_2 and NG/H_2 gas mixtures under 100 bar of gas mixture and 20 bar of partial H_2 pressure (the total pressure of the gas mixture was 100 bar to fix the H_2 partial pressure at the level of 20 bar of H_2 in all the experiments).

The hydrogenation was performed under isothermal conditions at 350 °C (for three h), followed by cooling to 215 or 195 °C (in 30 minutes). The only exception (regarding the hydrogenation time) was the first hydrogenation, where 24 h absorption was performed. Fig. S9† shows that the main part of the hydrogenation process is completed within half an hour. Nevertheless, to ensure the completion of the reaction, hydrogenation lasted for at least 3 hours in each hydrogenation/dehydrogenation cycle. The cooling was carried out by only heat losses to the environment, and no active cooling system was used. At each cycle, the hydrogenation was accomplished with the autoclave opened to the gas bottle for the entire process – which ensured an unlimited supply of H_2 necessary to reach full hydrogen storage capacity. Carrying out hydrogenation with the autoclave opened to the gas bottle also reflects the constant hydrogen content that can be expected in H_2 separation flow reactors.

After each hydrogenation process (when the autoclave was cooled to 215 or 195 °C), the gas remaining in the setup was vented, and the setup was five times purged using an alternately dynamic vacuum and 5 bar Ar. The autoclave with the hydrogenated material was then closed (through the valve), and the rest of the system was evacuated under a dynamic vacuum for one hour.

The dehydrogenation was performed in a part of the setup restricted to the autoclave and reservoir. In this case, the presence of a reservoir allowed for a significant increase in the system's volume during the H_2 desorption. It ensures that the rise of the pressure induced by the desorbed gas will not be too great, and the final pressure will not get close to the equilibrium one (at the dehydrogenation temperature) before dehydrogenation is completed. At the same time, the overall volume of the setup (composed of the autoclave and reservoir) is not too big, so the pressure change in the system is measurable with good precision – which allows us to calculate the amount of the desorbed gas and, therefore, the hydrogen storage capacity. The dehydrogenation process consisted of heating to 350 °C (in 30 minutes), followed by three hours of isothermal heating at the final temperature. The amount of the desorbed H_2 was calculated based on the change of the pressure in the known volume of the temperature-stabilized setup. After finishing the H_2 desorption, the dehydrogenated gas was expanded to the empty gas sampling bag for GC experiments.

After each dehydrogenation and before the following hydrogenation, the entire system was vented and degassed using a dynamic vacuum. After the final separation experiments, the autoclave was cooled to room temperature, and the materials in the hydrogenated state were transferred inside the autoclave to the glovebox to be further analyzed. All the samples were then studied using X-ray diffractometry (XRD), thermogravimetry (TG), differential scanning calorimetry (DSC), scanning electron microscopy (SEM), and energy dispersive X-ray spectroscopy (EDX).

Separation of H_2 from H_2/CO_2 gas mixture

Mg-Ni and Mg-Fe systems (0.3 g) were used to separate H_2 from the H_2/CO_2 gas mixture (99 : 1). In these experiments, a simplified setup was used (no gas reservoir; 26 mL autoclave). The material handling, degassing of the system, and hydrogenation/dehydrogenation temperatures were the same as described above. Before the separation experiments, each material was activated five times under pure H_2. The hydrogenation in the H_2/CO_2 gas mixture was performed under 50 bar total pressure in a closed autoclave (at approx. 0.5 bar CO_2 partial pressure).

Due to the slow kinetics of the process, the hydrogenation lasted at least 36 hours until the pressure in the autoclave was equilibrated. The hydrogenation/dehydrogenation cycles in an H_2/CO_2 gas mixture were performed four times for both studied systems. The gas left after hydrogenation and the desorbed gases were tested by GC.

GC

The gas samples collected at different stages of the gas separation process (leftover gas mixtures after absorption or desorbed gas) were studied with a gas chromatograph Agilent 6850 Network GC System with a thermal conductive detector. The chromatograph was equipped with a 27 m long PLOT capillary pillar with a diameter of 0.53 mm made of fused silica. The carrier and detector gas was N_2. To study the gas composition, the inlet of the GC was heated up to 220 °C, and the carrier inner gas flow was 1.7 mL min^{-1}. The average velocity inside the pillar (at 80 °C) was kept for 5 min at a level of 21 cm s^{-1}. The gas samples were transported inside the gas sampling bag and measured immediately after the sampling. For each gas mixture, three measurements were done.

XRD

The crystal structures and phase compositions of the starting materials, as-prepared and hydrogenated Mg-Ni and Mg-Fe systems, were evaluated using an X-ray powder diffractometer. The diffraction patterns were detected on an STOE STADI P transmission diffractometer. In all experiments, Mo radiation (0.7093 Å) was used. The instrument was equipped with a primary Ge (111) monochromator ($MoK\alpha_1$) and a position-sensitive Mythen1K detector. The data were collected between 5 and 70° 2θ with a step width of 0.015° 2θ. Measuring times per step was 20 s. For each measurement, eight scans were collected and summed after data collection. For the measurements, the samples were filled into borosilicate glass capillaries (0.3 or 0.5 mm outer diameter, 0.01 mm wall thickness) inside a glovebox and sealed afterwards. The measured diffractograms were compared with simulated data using the crystal structure data from the ICSD database.[46] The Rietveld refinement was performed using TOPAS Version 6 (Bruker AXS, Karlsruhe, Germany).[47]

DSC/TG/MS

The desorption of H_2 from the hydrogenated Mg-Ni and Mg-Fe systems (after a series of H_2 separation experiments) was studied using Mettler Toledo TGA/DSC 1 STARe System thermogravimetric differential scanning calorimetry. All experiments were conducted on ~15 mg of material placed inside a 40 μL Al sample crucible and run under 50 mL min^{-1} Ar gas flow. The heating was performed at 10 °C min^{-1} up to 480 °C. In several cases, the DSC/TG gas outlet was connected to the ThermoStar GSD 300 T2 mass spectrometer (MS) to record the gas desorption profiles (H_2 and CH_4) during the heating process. MS was also used to evaluate the composition of used NG.

SEM/EDX

The hydrogenated Mg-Ni and Mg-Fe systems were examined by scanning electron microscopy (SEM) – TM3030 (with an accelerating voltage of 15 kV) and Hitachi S-5500 (with an accelerating voltage of 30 kV). The chemical composition of the sample and distribution of elements were evaluated using Energy Dispersive X-ray Analysis (EDX) – Xplore Compact 30 (Oxford) and Thermo Scientific UltraDry (SSD). The samples were placed on a copper grid with a lacey (carbon) film or an aluminum stub with a Leit-Tab (carbon and sulfur). EDX was primarily used to determine the concentrations and distributions of Mg, Fe, and Ni, but it also allowed us to detect F, Si, and Ca traces (which were the impurities coming from the starting materials; not shown here).

Results and discussion

Separation of H_2 from CH_4-rich gas mixtures

Mg-Ni and Mg-Fe systems were used to separate H_2 from the CH_4/H_2 and NG/H_2 gas mixtures. In the first place, the accomplishment of the separation was evaluated based on the amount of desorbed H_2.

The evolution of the hydrogen storage capacity of the Mg-Ni system in the cycles (hydrogenation/dehydrogenation) of separation from different gas mixtures and at different starting desorption temperatures is presented in Fig. 1a. The hydrogen storage capacity measured after hydrogenation in pure H_2 was determined at the level of 5.41(13) wt%. Further experiments proved that the Mg-Ni system can separate H_2 well from CH_4/H_2 and NG/H_2 gas mixtures, reaching 5.44(17) and 4.86(35) wt% H_2, respectively.

The hydrogen desorption capacity related to the separation of H_2 from the CH_4/H_2 gas mixture is maintained on the same level as in experiments with pure H_2. It means that the Mg-Ni system can effectively separate H_2 from the gas mixtures dominated by CH_4 (an 80 : 20 gas mixture was used here). Moreover, surrounding the material with CH_4 does not hinder H_2 absorption or cause any side reactions that affect the separation capability.

Despite good separation abilities, a slight reduction of H_2 storage capacity and capacity deviations were observed for the experiments employing the NG/H_2 gas mixture. There are at least two plausible reasons for this phenomenon. The first is the partial poisoning of the Mg-Ni system by NG contaminations (CO_2 and H_2S – see Table S1 and Fig. S5†). The second is related to the partial instability of the Mg-Ni-based hydride at 215 °C. It is possible that because of the cycled hydrogenation/dehydrogenation, the kinetic of H_2 desorption was improved, and part of the stored H_2 was removed from the material during the system's purging (which was always performed after hydrogenation). The amount of H_2 desorbed from Mg-Ni system under isothermal conditions is presented in Fig. S10 and discussed in Chapter S5 of the ESI†.

To check whether the second explanation is at least partially responsible for the H_2 capacity reduction, we performed a series of dehydrogenation experiments starting at a reduced

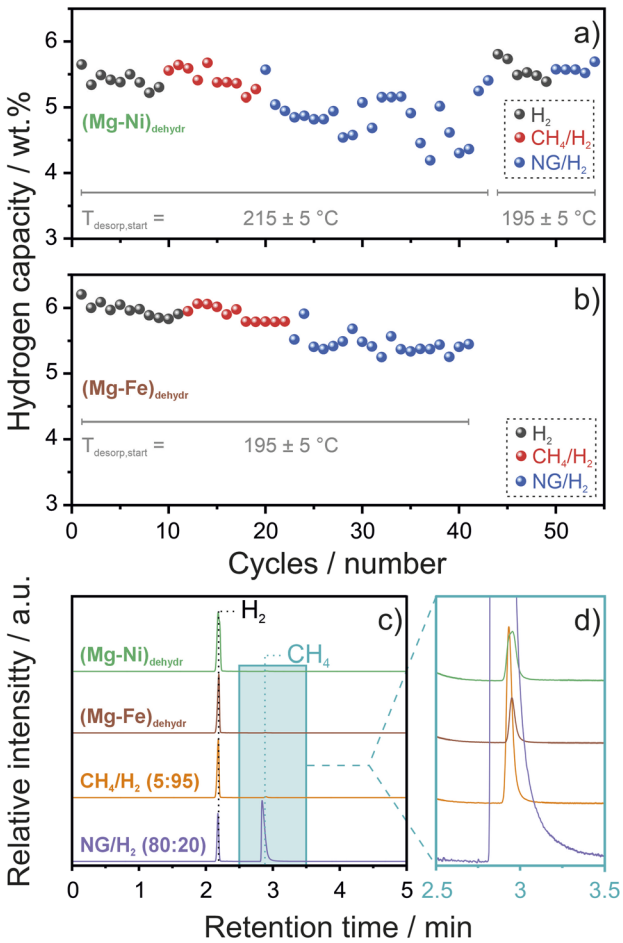

Fig. 1 H_2 storage capacity (measured during the desorption starting at 215 or 195 °C) as a function of hydrogenation/dehydrogenation cycles performed on (a) Mg-Ni (b) Mg-Fe systems. The hydrogenation has been performed under 20 bar H_2 (labeled as H_2), 100 bar of CH_4/H_2 gas mixture (20 bar of partial H_2 pressure, labeled as CH_4/H_2), and 100 bar of natural gas/H_2 gas mixture (20 bar of partial H_2 pressure, labeled as NG/H_2). The accuracy of measured capacities is close to 0.05 wt%. (c and d) results of GC made on the natural gas/H_2 gas mixture (20% H_2, labeled as NG/H_2), reference CH_4/H_2 gas mixture (95% H_2, labeled as CH_4/H_2), gas desorbed from the Mg-Ni and Mg-Fe systems after hydrogenation under 100 bar of NG/H_2 gas mixture (20 bar of partial H_2 pressure, labeled as $(Mg\text{-}Ni)_{dehydr}$ and $(Mg\text{-}Fe)_{dehydr}$, respectively). The dotted lines indicate the position of H_2 and CH_4 peaks. The blue area in (c) points out the region of patterns enlarged in (d).

temperature of 195 °C (Fig. 1a). The results show that by lowering the starting desorption temperature (and therefore the purging temperature), the H_2 desorption capacity was restored at the level of 5.57(16) wt% H_2 after hydrogenation in pure H_2. The following separation of H_2 from the NG/H_2 gas mixture did not cause a reduction in the storage capacity, which was recorded over cycling at the level of 5.59(6) wt%. This equals to ~59 mg H_2 desorbed from Mg-Ni system. It proves that purging/evacuating temperatures, which are directly related to the transition temperature between hydrogenation and dehydrogenation, are an essential factor to consider when designing the overall gas separation process.

Taking advantage of the optimization of the processing temperature for the Mg-Ni system, the separation properties of the Mg-Fe system were evaluated at the desorption starting temperature equaled to 195 °C. Similarly to Mg-Ni, the Mg-Fe system, exhibited good H_2 separation properties (Fig. 1b). The hydrogen storage capacity was maintained after switching the gas from pure H_2 to the CH_4/H_2 gas mixture. The capacities equaled 5.97(11) and 5.90(12) wt% for H_2 and CH_4/H_2 gas mixture, respectively. The Mg-Fe system was also able to separate 4.86(35) wt% H_2 when exposed to NG/H_2 gas mixture. This equals to ~51 mg H_2 desorbed from Mg-Fe system. The decrease in H_2 storage capacity observed after changing the gas mixture from CH_4/H_2 to NG/H_2 should be associated with partial poisoning of the material with NG impurities (as discussed below).

The purity of separated H_2 was assessed using GC, based on the gas samples dehydrogenated from Mg-Ni and Mg-Fe systems. Fig. 1c and d presents the GC curves of the above-mentioned gases compared to the NG/H_2 (80 : 20) and standard CH_4/H_2 (5 : 95) gas mixtures (which were used as reference ones). Both gas samples exhibit a high H_2 purity of 99.9% (according to the calibration curves in Fig. S7†). The GC detected only traces of CH_4. To determine if the CH_4 molecules are adsorbed at the metal surface, we performed the same absorption/desorption experiment (the same temperatures, pressures, and heating/cooling regimes) under pure CH_4. After this experiment, we did not detect any CH_4, indicating the necessity of H_2 absorption/desorption processes in capturing the CH_4 traces. In another series of experiments, we tried to determine at what point, of MgH_2 to Mg transition, CH_4 is desorbed (*e.g.*, only at the beginning or at the end of the process). However, our analysis always showed traces of CH_4, indicating CH_4 desorption associated with the release of H_2. The complete removal of CH_4 traces was impossible by Ar purging and degassing under a dynamic vacuum.

To summarize, we prove that independently of the applied catalyst (Ni or Fe), Mg-based systems can effectively separate significant amounts of highly pure H_2 from CH_4/H_2 or NG/H_2 gas mixtures. Moreover, the importance of the processing temperature was highlighted. To further elucidate the processes that occurred during the H_2 separation, the hydrogenated Mg-Ni and Mg-Fe systems (after the last separation of H_2 from NG/H_2 gas mixtures) were transferred to the glovebox to pursue detailed examination.

Mg-Ni system after separation of H_2 from CH_4/H_2 and NG/H_2 gas mixtures

The macroscopic observation of the hydrogenated Mg-Ni system revealed significant material inhomogeneity. To facilitate further analysis, we determined five material layers/samples, which are graphically presented in a simplified manner in Fig. 2a. The layers' thicknesses shown in Fig. 2a (and later in Fig. 4a and 5e) do not reflect the actual ones. Moreover, despite the distinct nature of each layer, there were also gradual transitions between them. The differences in the color of the

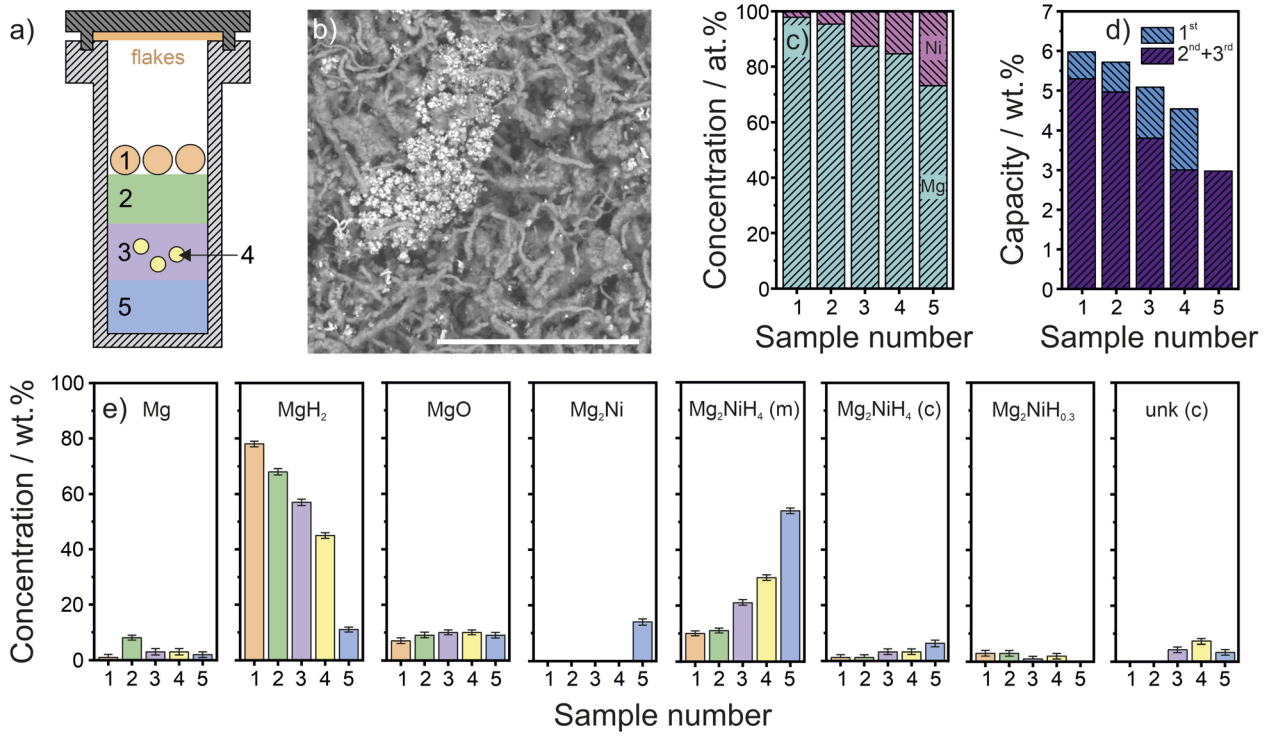

Fig. 2 (a) Scheme of the arrangement of the Mg-Ni system material after cycles of hydrogenation/dehydrogenation experiments under 20 bar H_2, 100 bar of CH_4/H_2 gas mixture (20 bar of partial H_2 pressure), and 100 bar of natural gas/H_2 gas mixture (20 bar of partial H_2 pressure). The numbers depict the positions of the layer/sample examined by different techniques; (b) BS-SEM image of the sample of 1st layer collected from the Mg-Ni system after cyclic experiments (at 15 kV). Scale bar: 100 μm; (c) the average concentration of Mg and Ni calculated based on the EDX results obtained for samples of different layers' collected from the Mg-Ni system after cyclic experiments; (d) hydrogen storage capacity determined from TG experiments on samples of different layers collected from the Mg-Ni system after cyclic experiments. Purple and blue bars show the amount of H_2 desorbed in the first (up to 305 °C) and jointly second and third steps of H_2 desorption (above 305 °C), respectively; (e) concentrations of different phases identified (*via* Rietveld refinement) for samples collected from various layers of the Mg-Ni system after cyclic experiments. The sample numbers in (c), (d), (e) correspond to those presented in scheme (a).

samples collected from different layers are presented in Fig. S12 and S13.†

Light grey granules formed the first layer. The granules were easy to fragment with a spatula. At the same time, they exhibit an elastic tendency to stay bulk and not disintegrate into a fine powder (which is typical for brittle metal hydrides). We also observed dark red spots that were present mainly on the granules' surface and rarely in their inner parts.

All subsequent layers were in the form of powder. The second layer had a slightly darker grey color than the first and only a few dark red spots were observed therein. The third layer, which consisted of the largest part of the Mg-Ni system material, had a greater share of the dark red spots. We separated some dark red spots from the third layer and labeled them fourth sample. The last, the fifth layer was located on the bottom of the autoclave and was composed of very dark red powder. Additionally, we observed very thin and brittle white flakes attached to the autoclave lid (resulted from Mg sublimation and condensation in the coolest spot of the autoclave).

The layers described above were further examined using SEM and EDX. Surprisingly, we discovered that the granules (first layer) mostly comprise networked microstructure (Fig. 2b and S14†). The interconnected rod-like structures were several μm in diameter and tens of μm in length. The detailed SEM analysis shows that they were composed of nanosized grains (Fig. S15†). This networked structure must be responsible for the aforementioned elastic nature of the granules. The previous studies demonstrated that Mg-MgH_2 system is represented by many nano and microstructures.[48] One of the examples are nanowhiskers formed during the hydrogen induced disproportionation of $Mg_{24}Y_5$.[49]

BS-SEM micrographs show the presence of additional, denser particles (bright part of the micrograph in Fig. 2b) of few μm in size. EDX analysis revealed that the networked structure consisted mainly of Mg, while the denser particles consisted of Mg and Ni (Fig. S16†).

The systematic analysis of SE- and BSE-SEM micrographs indicates that the share of Mg-Ni particles gradually increases with the number of subsequent layers to dominate over Mg particles in the fifth layer (Fig. S14†). Moreover, the networked microstructure visible in the first and second layers is mostly replaced by irregular Mg-based particles in the following layers. The change in the chemical composition of the following layers is clearly visible on EDX maps (Fig. S17†) and was summarized in Fig. 2c. The Ni concentration increased significantly from 2 to 27% between the first and fifth layers.

To investigate the influence of the observed chemical composition inhomogeneity on the hydrogen storage properties, the samples from all the layers were dehydrogenated using the DSC/TG apparatus. The DSC and TG curves show a multi-step H_2 desorption, manifested by endothermic events and corresponding materials weight loss (Fig. S18†). According to the literature, the first event (up to 305 °C) is related to the first step of Mg_2NiH_4 dehydrogenation.[50,51] The following, at least three, overlapping endothermic events (above 305 °C) correspond to further desorption of H_2 from Mg_2NiH_4 phase (the second and third step of its decomposition) and dehydrogenation of the MgH_2 phase.[50,52] The initial temperature of the second and main part of hydrogen desorption corresponds well to the H_2 desorption kinetic curve, which showed the main dehydrogenation occurs above 285 °C (Fig. S11†). The DSC curves analysis, revealing the presence of the Mg_2NiH_4 phase, which in a lattice distorted (microtwinned) form is characterized by an orange-rust color (which turns dark red upon the surface oxidation), corresponds well with macroscopic and SEM/EDX observations.[50] A decidedly different DSC curve shape, with a sharp endothermic event was observed for the sample from the fifth layer. According to E. Rönnebro *et al.*, this is related to the transformation of the distorted Mg_2NiH_4 phase from the low-temperature to high-temperature form, followed by rapid H_2 desorption (manifested in the DSC curve by the high-temperature shoulder of the peak).[50] The H_2 desorption of the fifth sample is completed by dehydrogenation of the MgH_2 phase (on-set temperature around 375 °C).

The total amount of H_2 desorbed during the DSC/TG experiments (4.5–5.93 wt% H_2; excluding the fifth layer, Fig. S18b†) fits well with the capacities reported in Fig. 1a. Fig. 2d summarizes the hydrogen desorption capacities of samples of different layers' in detail. The graph clearly shows that the overall H_2 storage capacity is decreased for the following layers. Moreover, the amount of H_2 desorbed from the material within the first endothermic event is increased from the first to the fourth sample. This trend is consistent with all previous observations of chemical separation: The MgH_2 phase, capable of storing up to 7.6 wt% H_2, is gradually replaced in the following layers of the material by less stable Mg_2NiH_4 phase capable of storing ~3.6 wt% H_2. This phenomenon ultimately results in the reduction of the hydrogen storage capacity and partial destabilization of the hydride. Moreover, the observed lower temperature stability of the Mg-Ni hydride (caused by the presence of the Mg_2NiH_4 phase) supports our conclusion of the necessity of lowering the starting dehydrogenation/system purging temperature (Fig. 1a).

As we presented in Fig. 1c and d the desorption of H_2 is accompanied by the desorption of CH_4 traces. To determine the period of CH_4 liberation, we analysed the gas desorbed from the DSC/TG apparatus with MS (Fig. S19†). The obtained curves show that CH_4 is desorbed at the same time as H_2, which confirms our previous observations. The amount of desorbed CH_4 is proportional to desorbed H_2.

CH_4 was not adsorbed on the metal-hydride particle surface as it could be easily removed from it by applying degassing under a dynamic vacuum and purging with Ar (see the discussion above). A mechanism based on the "hydride breathing" phenomenon is more likely. According to it, a small amount of a gas mixture (mainly CH_4) can be trapped in the pores of the MH particles, which close during hydrogenation (swelling of the active material) and open during dehydrogenation (contraction of the active material), releasing the trapped gas. Such a release process would strongly correlate to the H_2 desorption observed in this study. The change of the metal hydride porosity induced by the hydrogenation/dehydrogenation process was suggested by D. O. Dunikov *et al.* for $La_{0.9}Ce_{0.1}Ni_5$ alloy.[53]

The SEM analysis of the dehydrogenated sample (after DSC/TG experiments) from the first layer of the Mg-Ni system showed the complete stability of the Mg networked structure after the desorption process. This proves that hydrogen is not essential for stabilizing this microstructure (Fig. 3).

The further analysis focused on investigating the correlation of chemical inhomogeneity with the phase composition of subsequent material layers. It was determined based on the Rietveld refinement of the XRD patterns obtained for each layer's sample (Fig. 2e and S20†). The results revealed that most of the Mg-Ni system formed MgH_2, two Mg_2NiH_4 (monoclinic-m and cubic-c), and $Mg_2NiH_{0.3}$ hydride phases upon hydrogenation under the gas mixtures. In subsequent layers of the material, a tendency for MgH_2 to be replaced by both Mg_2NiH_4 phases was observed. This agrees with the discussion of the SEM/EDX and DSC/TG results and is consistent with the observed change in the color of following layers of the material. Chemical and phase segregation occurring in successive layers of the material result from differences in phase densities (1.74 and 3.28 g cm^{-3} for Mg and Mg_2Ni, respectively) and is induced by repeated severe volume expansion and contraction of the Mg-Ni system during the hydrogenation/dehydrogenation cycling (~30%).[54] The material volume change accompanied by gas flows resulted in particle mobility. This caused the heavier Ni-containing particles to gradually settle to the bottom of the autoclave.

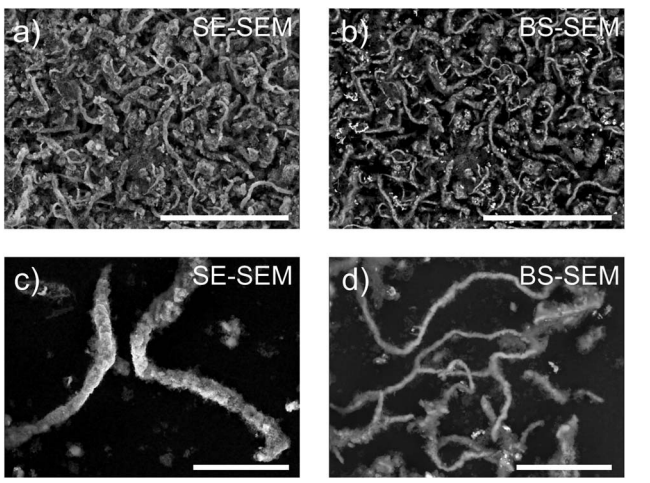

Fig. 3 SE-SEM (a and c) and BS-SEM (b and d) of the dehydrogenated (under TG/DSC experiment, 10 °C min^{-1}) 1st layer' sample (Fig. 2a) collected from the Mg-Ni system after cyclic separation experiments (15 kV). Scale bars: 100 μm (a and b), 30 μm (c and d).

Approximately 9 wt%. of MgO was detected in all hydrogenated Mg-Ni system layers. The MgO phase is formed due to the side reaction of Mg with NG impurities (as discussed below), and its presence negatively affects the system's hydrogen storage capacity. The Rietveld analysis did not detect any carbon-containing compounds, which proves that the Mg-Ni system did not react with CH_4 (the main component of NG). The same conclusion was reached in the past by B. Bogdanović *et al.*[39]

In summary, the results of the complementary techniques proved the chemical and phase composition inhomogeneity in the hydrogenated Mg-Ni system after H_2 separation cycling. The relatively light, Mg-rich surface layer is gradually enriched in denser Ni-containing phases while moving to lower material layers. The described phase and chemical composition gradients also affect the hydrogen storage capacity of each material layer. The inhomogeneity and partial material poisoning (formation of the MgO phase) do not affect the system's ability to separate pure H_2 from gas mixtures.

Mg-Fe system after separation of H_2 from CH_4/H_2 and NG/H_2 gas mixtures

After the series of gas separation experiments, the hydrogenated Mg-Fe system was evaluated in the same way as the Mg-Ni system. The macroscopic observation revealed material inhomogeneity and the formation of four material layers, which are graphically presented in Fig. 4a and S21.† The upper layer consisted of several light grey and brittle granules, which, did not exhibit the elastic nature of the granules observed in the Mg-Ni system. In subsequent layers, the light grey powder gradually darkened, and rare reddish material spots appeared, the concentration of which continuously increased. Moreover, unlike the Mg-Ni system, no brittle flake layer attached to the lid was observed in the Mg-Fe system.

The EDX and SEM results showed a gradual increase in Fe concentration in subsequent layers of the material (Fig. 4b, S22, and S23†). However, the differences in Fe concentration between the layers are less explicit than in the case of Ni in the Mg-Ni system. SEM images revealed that the hydrogenated Mg-Fe system consists of irregular Mg-based particles of tens of μm in diameter and denser Fe-rich particles of a few μm in diameter (brighter parts in BS-SEM images) – see Fig. 4c and S23.† The detailed SEM analysis showed that the Mg-based particles were intensely fractured after the cycled separation experiments (Fig. 4d and S23†). Since no networked Mg-based microstructure was observed in the Mg-Fe system, its formation must be associated with the presence of Ni in the Mg-Ni system.

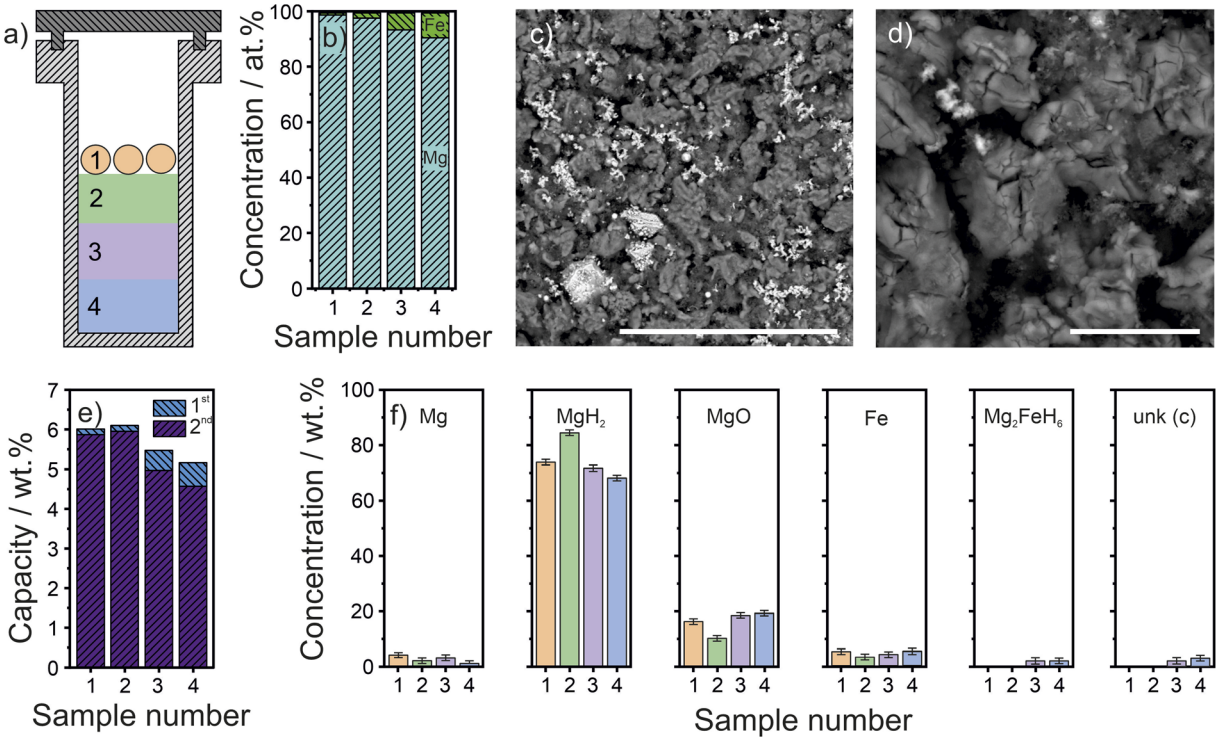

Fig. 4 (a) Scheme of the arrangement of the Mg-Fe system material after cycles of hydrogenation/dehydrogenation experiments under 20 bar H_2, 100 bar of CH_4/H_2 gas mixture (20 bar of partial H_2 pressure), and 100 bar of natural gas/H_2 gas mixture (20 bar of partial H_2 pressure). The numbers depict the positions of the layer/sample examined by different techniques; (b) the average concentration of Mg and Fe calculated based on the EDX results obtained for samples of different layers' collected from the Mg-Fe system after cyclic experiments; (c and d) BS-SEM images of the sample of 3rd layer collected from the Mg-Fe system after cyclic experiments (all at 15 kV). Scale bars: 100 μm (c) and 10 μm (d); (e) hydrogen storage capacity determined from TG experiments on samples of different layers collected from the Mg-Fe system after cyclic experiments. Purple and blue bars show the amount of H_2 desorbed in the first (up to 350 °C) and in the second step of H_2 desorption (above 350 °C), respectively; (f) concentrations of different phases identified (*via* Rietveld refinement) for different layers' samples collected from the Mg-Fe system after cyclic experiments.

The DSC/TG analysis shows two well-separated endothermic dehydrogenation events for each sample collected from the hydrogenated Mg-Fe system (Fig. S24†). The first event, in the range of 250–350 °C, corresponds to the desorption of H_2 from Mg_2FeH_6.[55] The second event, with an onset temperature of approximately 350 °C, manifested by a clearly visible endothermic reaction, is related to the dehydrogenation of the MgH_2. The share of the first event in the overall dehydrogenation storage capacity is increased for the subsequent layers. However, the differences in the capacity between layers are not as pronounced as in the Mg-Ni system, suggesting better resistance to chemical and phase segregation in the Mg-Fe system than in the Mg-Ni system (Fig. 4e). The dehydrogenation storage capacities (5.16–6.10 wt% H_2, Fig. 4e) corresponds well to the ones presented in Fig. 1b. The DSC/TG results agree with SEM/EDX and macroscopic observations which revealed a higher Fe concentration in subsequent layers and a darkening of the powder color. Mg_2FeH_6 particles, which are green, mixed with light grey MgH_2 particles cause a darkening of the powder, the final shade of which depends on the proportion of both hydride phases.

XRD analysis of samples from different layers confirmed that most of the Mg in the Mg-Fe system formed the MgH_2 phase upon separation experiment (Fig. 4f and S25†). Moreover, the Rietveld analysis confirmed that Fe only slightly separated between the layers. The larger amount of Mg_2FeH_6 (detectable by XRD) was confirmed only for the third and fourth layers. This fits well with the larger weight loss associated with the first dehydrogenation event (up to 350 detected °C) in the DSC/TG curves. However, most of the Fe did not react with Mg to form a hydride phase and remains metallic Fe. The Rietveld refinement also pointed to the relatively high concentration of MgO (10–20 wt%), which, as in the case of the Mg-Ni system, originates from poisoning inducted by NG impurities (as discussed below). The rare reddish spots observed macroscopically may be related to the formation of Fe_2O_3, the presence of which, however, due to its low concentration, was not confirmed by XRD analysis.

Although the results of complementary techniques showed chemical and phase segregation in the Mg-Fe system (after the cycled H_2 separation experiments), the inhomogeneity was not as severe as in the case of the Mg-Ni system. Moreover, the detected inhomogeneity and partial material poisoning did not affect the ability of the Mg-Fe system to separate pure H_2 from gas mixtures.

The influence of CO_2 impurity on the hydrogen storage properties

The NG impurities considered harmful to metal hydrides include O_2, CO, CO_2, H_2O, SO_2, and H_2S. The impact of these impurities on low-temperature hydrides (AB_5- and AB-type systems) was addressed by G. D. Sandrock *et al.*[28] Our study showed that the separation of H_2 from NG/H_2 leads to poisoning of Mg-based systems, resulting in partial Mg oxidation and loss of hydrogen storage capacity. Therefore, the following part of our research focused on understanding the distinct impact of CO_2 impurity (according to Table S1 and Fig. S5,† the main pollutant of NG used here) on the hydrogen storage ability of Mg-based systems. For this reason, the activated Mg-Ni and Mg-Fe systems were hydrogenated four times in H_2/CO_2 gas mixture (99 : 1). To emphasize the possible poisoning phenomenon, a relatively high CO_2 concentration was chosen (two orders of magnitude higher than in used here NG).

The analysis of the pressure change associated with hydrogenation of both systems under H_2/CO_2 gas mixture shows that the presence of CO_2 significantly slows down the reaction kinetics (Fig. 5a). The total hydrogenation time was increased from three (used in experiments with NG/H_2 gas mixture) to 30–60 hours. Moreover, the hydrogenation took place in two steps. A decrease in hydrogenation kinetics without a change in hydrogen storage capacity is called retardation and was observed to be induced, for example, by an NH_3-containing gas mixture.[28] Our observation differs from the results reported by B. Bogdanović *et al.*, who observed no detrimental effect of 1% CO contamination (which reacts even more active with the metallic surface than CO_2) on the Mg-Ni system hydrogenation/dehydrogenation kinetics.[39]

The analysis of the gas leftover after the hydrogenation process revealed that all CO_2 present in the initial gas mixture was reduced to CH_4 (Fig. 5b–d). This reaction was catalyzed by Ni and Fe catalysts according to the following Sabatier reaction:

$$CO_2 + 4H_2 \rightleftarrows CH_4 + 2H_2O \quad (1)$$

The catalytic activity of Ni and Fe towards the methanation of CO and CO_2 has been studied elsewhere.[56]

As a result of this reaction, twice as many H_2O molecules are produced than CH_4. At the hydrogenation temperature (350 °C) used herein, the presence of H_2O vapor causes the observed oxidation of Mg. The heterogeneous CO_2 reduction reaction may also be partly responsible for the observed reduced hydrogenation kinetics. When Ni and Fe are used not only in the catalysis of the hydrogenation reaction but also in the reduction of CO_2, the hydrogenation rate is decreased. The following analysis of the gas desorbed from the metal hydride (Fig. 5b and c after dehydrogenation) confirmed that highly pure H_2 (with only traces of CH_4) is recovered from the material despite its partial poisoning.

After a series of hydrogenation experiments in H_2/CO_2 gas mixtures, the hydrogenated Mg-Ni and Mg-Fe systems were further studied by XRD and DSC/TG techniques. The macroscopic observations revealed that both Mg-based systems were homogeneous light gray powders (Fig. S26–S28). No dark red spots were observed. For the Mg-Ni system, an additional layer of light gray flakes was observed on the autoclave lid (the flakes were easy to fracture but did not immediately fall apart when touched).

The XRD analysis proved the assumed oxidation of the Mg in both systems (Fig. 5f and S29†). The Rietveld refinement of the XRD patterns showed that >60(4) wt% of the systems consist of the MgO phase, which indicates a severe impact of the poisoning process. As expected, the formation of stable MgO

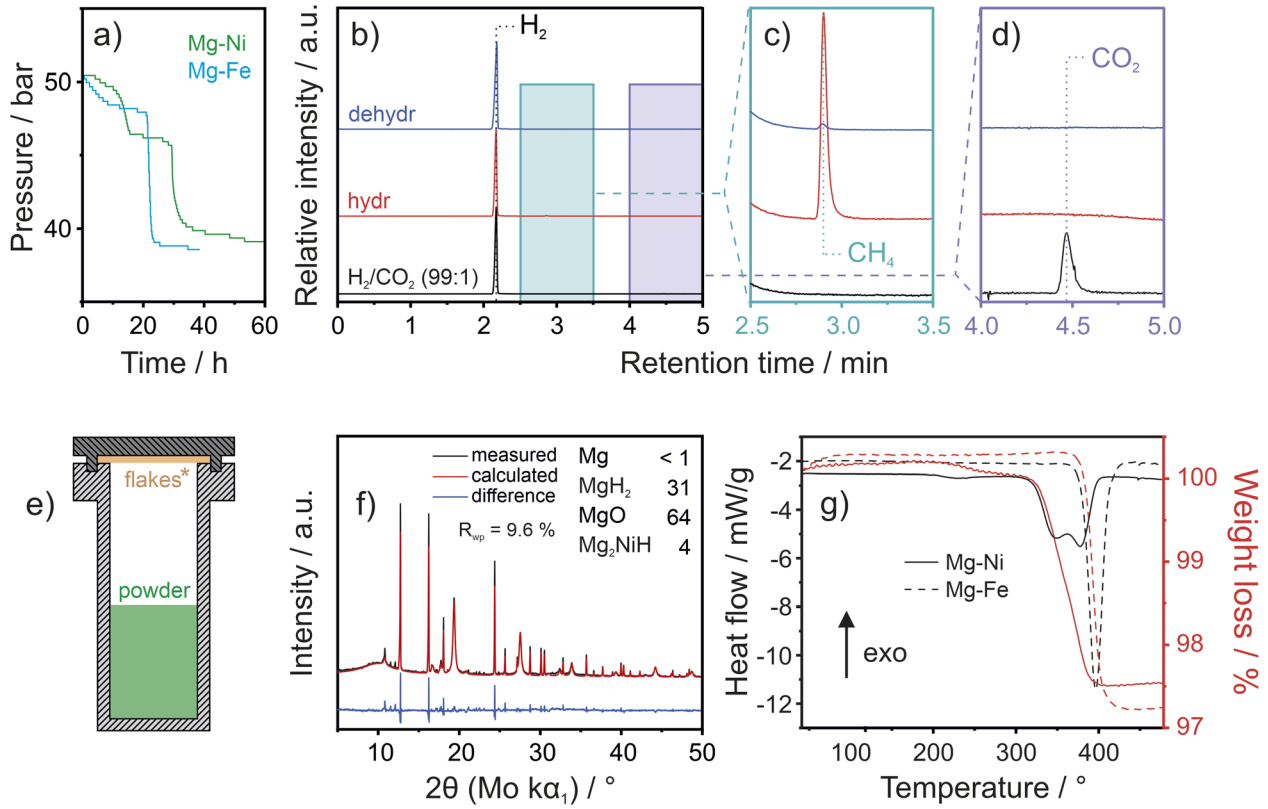

Fig. 5 (a) Change of the pressure during hydrogenation of activated Mg-based systems under ~50 bar of H_2/CO_2 gas mixture (0.5 bar of partial CO_2 pressure); (b–d) results of GC made on the: H_2/CO_2 gas mixture (1% CO_2, labeled as H_2/CO_2), leftover gas after the hydrogenation process (labeled as hydr), gas desorbed from the Mg-based systems after hydrogenation under ~50 bar of H_2/CO_2 gas mixture (0.5 bar of partial CO_2 pressure, labeled as dehydr). The dotted lines indicate the position of H_2, CH_4, and CO_2 peaks. The blue and purple areas in (b) point out the regions of patterns enlarged in (c) and (d), respectively; (e) scheme of the arrangement of the materials of Mg-based systems after four cycles of hydrogenation/dehydrogenation experiments under ~50 bar of H_2/CO_2 gas mixture (0.5 bar of partial CO_2 pressure). * indicates that flakes were detected only in the case of the Mg-Ni system; (f) XRD pattern and Rietveld refinement plot of the hydrogenated Mg-Ni system powder sample. The concentrations of the main phases are presented in wt%; (g) DSC and TG curves obtained for the hydrogenated Mg-based system powder samples (10 °C min^{-1}).

affected the hydrogen storage capability, resulting in a reduction in storage capacity that was approximately proportional to the MgO phase content in the hydrogenated system. The hydrogenated Mg-Ni and Mg-Fe system samples desorbed 2.51 and 2.76 wt% H_2, respectively (Fig. 5g). The decomposition of metal hydrides (conducted using the DSC method) was similar to the processes observed for the samples after H_2 separation experiments (Fig. 5g, S18 and S24†).

The formation of a surface MgO layer on the Mg-based particles at the beginning of the hydrogenation reaction is also partly responsible for the hydrogenation retardation. As observed for the $2LiNH_2 + MgH_2$ system, the presence of a surface oxide layer prevents diffusion of the atomic hydrogen into the metallic bulk.[42]

The overall analysis of the results of experiments using an H_2/CO_2 gas mixture shows that 1% CO_2 in H_2 is fatally hazardous to the hydrogenation storage properties of the Mg-based system (affecting the hydrogen storage capacity and reaction kinetics). The poisoning, however, does not affect the system's ability to separate pure H_2 (even if the amount of separated H_2 is significantly lowered).

Conclusions and outlook

In conclusion, we demonstrated that Mg-based systems can effectively separate large quantities of pure H_2 from CH_4-rich gas mixtures. The purity of recovered H_2 is not affected by observed material poisoning. Both tested hydrogenation catalysts, Ni and Fe, presented similar performance. We highlighted also the importance of proper selection of the processing temperature on the amount of recovered H_2 during dehydrogenation.

Moreover, this research provided unprecedented insights into processes taking place during H_2 separation – undescribed so far for any metal hydride. The results of complementary techniques exhibited partial chemical and phase segregation in the Mg-based system, which was, less prominent in the Mg-Fe than in the Mg-Ni system. Our study showed that homogenizing the chemical distribution of the active material before gas separation does not ensure its maintenance during this process. Nevertheless, no negative impact of observed segregation on the abilities of the Mg-based systems to separate pure H_2 was observed. The particle mobility during cycled separation

experiments can be significantly reduced by employing a binding material such as graphite. The addition of graphite not only immobilizes the metal particles but also increases the thermal conductivity of the material (which translates into more dynamic system operation).[57] The disadvantage of this solution is the reduction of the volumetric H_2 storage density of the separation system.

The awareness of the mentioned segregation, which certainly involves a change in the mass distribution inside the tested container, may be crucial when designing full-scale systems based on metal hydrides. This study shows that detailed post-processing analysis of the materials employed for H_2 separation/purification is crucial, even in systems as simple as Mg-Ni or Mg-Fe.

Interestingly, we presented the MgH_2 networked microstructure formation. We proved that this microstructure is stable after dehydrogenation.

Finally, we indisputably proved the fatal impact of CO_2 impurity on the hydrogen storage properties of the Mg-based systems. The formation of H_2O vapors accompanying the reduction of CO_2 to CH_4 causes the deactivation of Mg through its, at least surface, oxidation.

The use of MHs for the separation of H_2 from various gas mixtures undoubtedly requires solving this major issue. The origin of the poisoning may be related to a chemical reaction involving the active material, the catalyst, or both. An example of an active material-related origin of poisoning was discussed by F. Sun *et al.*, who reported a decrease in the H_2 desorption capacity and a decline of process kinetics in KF doped ($2LiNH_2 + MgH_2$) material upon hydrogenation in H_2/CO (1 mol% CO). In that case, carbon from CO reacted with Li^+, N^{3-}, and K^+ to cause permanent loss of the NH_2 groups of the active material and inactivation of the KF catalyst.[58] In contrast, in our study, the Mg-based system poisoning is caused by the presence of applied catalysts (Ni, Fe).

Prevention of poisoning in metal hydrides can be achieved through various approaches, offering potential solutions to this significant issue. One such approach is to use a different catalyst that enables the hydrogenation process to be carried out at a lower temperature and does not catalyze the CO_2 reduction reaction.[59] For instance, the CO_2 poisoning effect, although observed, was not severe in the case of AB_5-type systems operating below 100 °C.[29,30] The strong dependence of the CO_2 reduction reaction rate and its selectivity on the presence or absence of a catalyst, as well as the reaction parameters (temperature, time, *etc.*), was demonstrated by G. Amica *et al.* for the Mg-Co system.[60] Alternatively, the Mg-based system could be operated without a catalyst, but this would adversely affect the hydrogenation kinetics.

A promising approach is to modify the metal hydride surface with a protective layer that can separate gaseous species based on their molecular size (for example, employing the fluoride layer and aminosilane functionalization).[61,62] The improvement of the resistivity against CO and CO_2 poisoning for Mg-rich alloy was described by H. Wang *et al.*[63] Such a protective layer could be, however, ruptured during particle volume expansion and contraction that accompanies cyclic hydrogenation/dehydrogenation, resulting in an exposure of fresh, non-coated surface that could be poisoned.

Another solution involves an additional pre-purification system that eliminates severe pollutants (CO_2, O_2, H_2O, H_2S, CH_3SH) from the gas steam. The so-called natural gas sweetening plants are used as a standard purification unit eliminate sour compounds of natural gas such as CO_2 and H_2S.[64,65] The above-described phenomenon of Mg poisoning also requires looking at it from a different perspective. Because of the high CO_2 reactivity and full conversion of CO_2 into the CH_4, the Mg-based systems can be considered as potential candidates for the CO_2 capture and subsequent CH_4 conversion units.[66]

The further development of the Mg-based system should also lead to achieving an H_2 storage capacity close to the MgH_2 theoretical one. The robust MH-based system could be employed not only to separate H_2 from CH_4-rich gas mixtures but also, for example, to recover H_2 from waste gases from the semiconductor production,[67] from tail gases of NH_3 synthesis,[68] as well as to purify H_2 produced from NH_3 decomposition or biomass hydrothermal gasification.[69,70] Moreover, some alkaline fuel cells are considered to operate well when fed with CH_4/H_2 gas mixtures transported through NG pipelines.[19] The H_2 concentration in such gas mixtures could be adjusted by employing MHs.

Data availability

All the data supporting this article have been included as part of the ESI.†

Author contributions

M. Balcerzak: conceptualization, data curation, formal analysis, investigation, methodology, supervision, validation, visualization, writing – original draft, writing – review & editing. R. Urbanczyk: funding acquisition, supervision, writing – review & editing. F. Lange: data curation, investigation F. A. Helm: data curation, investigation J. Ternieden: investigation, data curation, writing – review & editing M. Felderhoff: funding acquisition, supervision, writing – review & editing. All authors have approved the final version of the manuscript.

Conflicts of interest

There are no conflicts to declare.

Acknowledgements

This project (IGF Vorhaben 20761 N) was funded by the German Federal Ministry of Economics and Energy on the basis of a resolution of the German Bundestag. The authors gratefully acknowledge the help of Dr. Özgül Agbaba, who provided standard gas mixtures for GC calibration, Felipe Marques, who provided SEM images of pure elements, and the scientists from the Chemical Crystallography and Electron Microscopy Department (SEM and EDX analysis) and the High-Pressure Laboratory. Open access funded by DEAL Project. Open Access funding provided by the Max Planck Society.

References

1 F. Kullmann, J. Linßen and D. Stolten, *Int. J. Hydrogen Energy*, 2023, **48**, 38936–38952.
2 Homepage of german Vereinigung der Fernleitungsnetzbetreiber Gas e.V. (FNB Gas), 14 March 2024, https://fnb-gas.de/en/hydrogen-core-network/.
3 S. Timmerberg and M. Kaltschmitt, *Appl. Energy*, 2019, **237**, 795–809.
4 Z. Du, L. Congmin, Z. Junxiang, G. Xiuying, X. Yalin, S. Wei and H. Guangli, *Catalysts*, 2021, **11**, 393.
5 M. Yáñez, F. Relvas, A. Ortiz, D. Gorri, A. Mendes and I. Ortiz, *Sep. Purif. Technol.*, 2020, **240**, 116334.
6 T. Yang, Y. Xiao and T.-S. Chung, *Energy Environ. Sci.*, 2011, **11**, 4171–4180.
7 R. Kumar, D. E. Guro and W. P. Schmidt, *Gas Sep. Purif.*, 1995, **9**, 271–276.
8 A. Golmakani, S. Fatemi and J. Tamnanloo, *Sep. Purif. Technol.*, 2017, **176**, 73–91.
9 R. R. Sadhankar, C. R. Aelick, D. L. Burns and K. Marcinkowska, *Can. J. Chem. Eng.*, 2000, **78**, 1087–1095.
10 Z. Wu, Z. Zhang and M. Ni, *Energy Convers. Manage.*, 2018, **174**, 802–813.
11 L. Dehdari, P. Xiao, K. Gang Li, R. Singh and P. A. Webley, *Chem. Eng. J.*, 2022, **450**, 137911.
12 D. Werner, *Chem. Ing. Tech.*, 1981, **53**, 73–81.
13 G. C. Bandlamudi, M. Wetergrove, L. N. Warr, J. Wartmann and A. Kruth, *Energy Technol.*, 2024, 2301023.
14 H. Fan, A. Mundstock, A. Feldhoff, A. Knebel, J. Gu, H. Meng and J. Caro, *J. Am. Chem. Soc.*, 2018, **140**, 10094–10098.
15 S. Kämnitz, A. Simon, H. Richter, M. Weyd, U. Lubenau, T. Geisler and I. Voigt, *Chem. Ing. Tech.*, 2022, **94**, 49–55.
16 D. V. Strugova, M. Yu Zadorozhnyy, E. A. Berdonosova, M. Yu Yablokova, P. A. Konik, M. V. Zheleznyi, D. V. Semenov, G. S. Milovzorov, M. Padaki, S. D. Kaloshkin, V. Yu Zadorozhnyy and S. N. Klyamkin, *Int. J. Hydrogen Energy*, 2018, **43**, 12146–12152.
17 K. Wagner, P. Tiwari, G. F. Swiegers and G. G. Wallace, *Adv. Energy Mater.*, 2018, **8**, 1702285.
18 A. Abdulla, K. Laney, M. Padilla, S. Sundaresan and J. Benziger, *AIChE J.*, 2021, **57**, 1767–1779.
19 K. Wagner, P. Tiwari, G. F. Swiegers and G. G. Wallace, *Energy Environ. Sci.*, 2018, **11**, 172–184.
20 S. Mrusek, M. Blasius, F. Morgenroth, S. Thiele and P. Wasserscheid, *Int. J. Hydrogen Energy*, 2024, **50A**, 526–538.
21 D. Dunikov, V. Borzenko and S. Malyshenko, *Int. J. Hydrogen Energy*, 2012, **37**, 13843–13848.
22 S. S. Hashim, M. R. Somalu, K. S. Loh, S. Liu, W. Zhou and J. Sunarso, *Int. J. Hydrogen Energy*, 2018, **43**, 15281–15305.
23 S. Yun and S. T. Oyama, *J. Membr. Sci.*, 2011, **375**, 28–45.
24 W. Liemberger, M. Gross, M. Miltner, H. Prazak-Reisinger and M. Harasek, *Chem. Eng. Trans.*, 2016, **52**, 427–432.
25 P. S. O. Patrício, J. A. de Sales, G. G. Silva, D. Windmöller and J. C. Machado, *J. Membr. Sci.*, 2006, **271**, 177–185.
26 D. Wang, W. K. Teo and K. Li, *J. Appl. Polym. Sci.*, 2002, **86**, 698–702.
27 B. Li, G. He, X. Jiang, Y. Dai and X. Ruan, *Front. Chem. Sci. Eng.*, 2016, **10**, 255–264.
28 G. D. Sandrock and P. D. Goodell, *J. Less-Common Met.*, 1984, **104**, 159–173.
29 A. Kumar and P. Muthukumar, *Int. J. Hydrogen Energy*, 2023, **48**, 37774–37783.
30 N. Hanada, T. Nakagawa, H. Asada, M. Ishida, K. Takahashi, S. Isobe, I. Saita, K. Asano, Y. Nakamura, A. Fujisawa and S. Miura, *J. Alloys Compd.*, 2015, **647**, 198–203.
31 M. Au, C. Chen, Z. Ye, T. Fang, J. Wu and O. Wang, *Int. J. Hydrogen Energy*, 1996, **21**, 33–37.
32 T. Saitou and K. Sugiyama, *J. Alloys Compd.*, 1995, **231**, 865–870.
33 F. R. Block and H.-J. Bahs, *J. Less-Common Met.*, 1983, **89**, 77–84.
34 S. Bouaricha, J. Huot, D. Guay and R. Schulz, *Int. J. Hydrogen Energy*, 2002, **27**, 909–913.
35 D. E. Dedrick, R. Behrens and R. W. Bradshaw, *Sandia Report, SAND2007-4960*, Sandia National Laboratories. s.l., 2007. https://www.osti.gov/biblio/920782.
36 C.-C. Shen and H.-C. Li, *Int. J. Hydrogen Energy*, 2015, **40**, 3277–3282.
37 13 March 2024, https://www.argusmedia.com/en/news-and-insights/latest-market-news/2547490-eu-magnesium-prices-enter-grey-area-below-3-000-t.
38 B. Bogranović, *US Pat.*, Nr. 4,749,558, 1988.
39 B. Bogdanović and B. Spliethoff, *Int. J. Hydrogen Energy*, 1987, **12**, 863–873.
40 S. Ono, Y. Ishida, E. Akiba, K. Jindo, Y. Sawada, I. Kitagawa and T. Kakutni, *Int. J. Hydrogen Energy*, 1986, **11**, 381–387.
41 A.-L. Woeste, M. Balcerzak, R. Urbanczyk and M. Felderhoff, *Energy Technol.*, 2021, **9**, 2001079.
42 G. Liang, J. Huot, S. Boily, A. Van Neste and R. Schulz, *J. Alloys Compd.*, 1999, **292**, 247–252.
43 H. Liang, H. Zhang, Y. Zong, H. Xu, J. Luo, X. Liu and J. Xu, *J. Alloy Compd.*, 2022, **905**, 164279.
44 L. Zhang, L. Ji, Z. Yao, N. Yan and Z. Sun, *Int. J. Hydrogen Energy*, 2019, **44**, 21955–21964.
45 F. Sun, M.-Y. Yan, X.-P. Liu, J.-H. Ye and Z.-N. Li, *Int. J. Hydrogen Energy*, 2015, **40**, 6173–6179.
46 D. Zagorac, H. Muller, S. Ruehl, J. Zagorac and S. Rehme, *J. Appl. Crystallogr.*, 2019, **52**, 918–925.
47 A. A. Coehlo, *J. Appl. Crystallogr.*, 2018, **51**, 210–218.
48 C. Zhu, S. Hosokai, I. Matsumoto and T. Akiyama, *Cryst. Growth Des.*, 2010, **10**, 5123–5128.
49 C. Zlotea, J. Lu and Y. Andersson, *J. Alloys Compd.*, 2016, **426**, 357–362.
50 E. Rönnebro and D. Noréus, *Appl. Surf. Sci.*, 2004, **228**, 115–119.
51 J. Zhang, D. W. Zhou, L. P. He, P. Peng and J. S. Liu, *J. Phys. Chem. Solids*, 2009, **70**, 32–39.
52 J. Čermák and L. Král, *Acta Mater.*, 2008, **56**, 2677–2686.
53 D. O. Dunikov, D. V. Blinov, A. M. Bozieva, A. N. Kazakov, A. A. Krapivina, I. A. Romanov, E. V. Zadneprovskaya and S. I. Allakhverdiev, *Int. J. Hydrogen Energy*, 2024, **51**, 375–387.

54 K. Nogita, X. Q. Tran, T. Yamamoto, E. Tanaka, S. D. McDonald, C. M. Gourlay, K. Yasuda and S. Matsumura, *Sci. Rep.*, 2015, **5**, 8450.
55 M. Polanski, T. K. Nielsen, Y. Cerenius, J. Bystrzycki and T. R. Jensen, *J. Hydrogen Energy*, 2010, **35**, 3578–3582.
56 S. De, J. Zhang, R. Luque and N. Yan, *Energy Environ. Sci.*, 2016, **9**, 3314–3347.
57 M. Lau, O. Ehrensberger, T. Weißgärber and F. Heubner, *Int. J. Hydrogen Energy*, 2024, **71**, 562–570.
58 F. Sun, M.-Y. Yan, J.-H. Ye, X.-P. Liu and L.-J. Jiang, *J. Alloys Compd.*, 2014, **616**, 47–50.
59 F. J. Antiqueira, D. R. Leiva, G. Zepon and W. J. Botta, *Int. J. Hydrogen Energy*, 2022, **47**, 470–489.
60 G. Amica, S. Rozas Azcona, S. Aparicio and F. C. Gennari, *Phys. Chem. Chem. Phys.*, 2020, **22**, 14720–14730.
61 M. V. Lototsky, M. Williams, V. A. Yartys, Ye. V. Klochko and V. M. Linkov, *J. Alloys Compd.*, 2011, **509S**, S555–S561.
62 M. Lototskyy, K. D. Modibane, M. Williams, Ye. Klochko, V. Linkov and B. G. Pollet, *J. Alloy. Compd.*, 2013, **580**, S382–S385.
63 H. Wang, Y. Liu and J. Zhang, *Adsorption*, 2022, **28**, 85–95.
64 M. Mohajeri, M. Panahi and A. Shahsavand, *Comput. Chem. Eng.*, 2024, **184**, 108631.
65 A. Baudot, Natural Gas Sweetening, in *Encyclopedia of Membranes*, ed. E. Drioli and L. Giorno. Berlin Heidelberg: Springer-Verlag, 2012.
66 M. L. Grasso, J. Puszkiel, F. C. Gennari, A. Santoru, M. Dornheim and C. Pistidda, *Phys. Chem. Chem. Phys.*, 2020, **4**, 1944–1952.
67 L. Rochlitz, M. Steinberger, R. Oechsner, A. Weber, S. Schmitz, K. Schillinger, M. Wolff and A. Bayler, *Int. J. Hydrogen Energy*, 2019, **44**, 17168–17184.
68 R. T. Abudu, Q. Sun, Z. Xu, X. Guo and L. Yang, *J. Chem. Eng. Data*, 2020, **65**, 1715–1720.
69 L. Lin, Y. Tian, W. Su, Y. Luo, C. Chen and L. Jiang, *Sustainable Energy Fuels*, 2020, **4**, 3006–3017.
70 M. Holewa, R. Dürrschnabel, N. Boukis and P. Pfeifer, *Int. J. Hydrogen Energy*, 2018, **43**, 13294–13304.

